DFNE 18– 0151_0228_000600

Pre- and Post-Blast Rock Block Size Analysis Using UAV-based Data and Discrete Fracture Network

Medinac, F., Bamford, T. and Esmaieli, K.
Lassonde Institute of Mining, University of Toronto, ON, Canada
Schoellig, A. P.
University of Toronto Institute for Aerospace Studies (UTIAS), Toronto, ON, Canada

ABSTRACT: Drilling and blasting is one of the key processes in open pit mining, required to reduce in-situ rock block size to rock fragments that can be handled by mine equipment. It is a significant cost driver of any mining operation which can influence the downstream mining processes. In-situ rock block size influences the muck pile size distribution after blast, and the amount of drilling and explosive required to achieve a desired distribution. Thus, continuous measurement of pre- and post-blast rock block size distribution is essential for the optimization of the rock fragmentation process.

This paper presents the results of a case study in an open pit mine where an Unmanned Aerial Vehicle (UAV) was used for mapping of the pit walls before blast. Pit wall mapping and aerial data was used as input to generate a 3D Discrete Fracture Network (DFN) model of the rock mass and to estimate the in-situ block size distribution. Data collected by the UAV was also used to estimate the post-blast rock fragment size distribution. The knowledge of in-situ and blasted rock size distributions can be related to assess blast performance. This knowledge will provide feedback to production engineers to adjust the blast design.

1. INTRODUCTION

A rock mass has naturally occurring joints, characterized by orientation, persistence, frequency and surface geometry (Grenon et al., 1998). The intersections of these joints create blocks of intact rock within the rock mass which determine the in-situ block size distribution (IBSD) (Elmouttie and Poropat, 2011). It is possible to obtain many of these joint properties using mapping; however, the three-dimensional nature of joint geometry poses a challenge (Dershowitz and Einstein, 1988). Another limitation includes manual mapping of inaccessible areas, particularly for open pit mines where once a bench has been fully excavated, there is no further access for wall mapping of that bench. As observed by Francioni et al., 2015, relatively few published papers have addressed the application of Unmanned Aerial Vehicles (UAVs) for joint mapping; however, they are becoming an increasingly popular method for overcoming this limitation. The additional data made available by UAVs is used to complement the information gathered through manual wall mapping techniques, thus providing a more extensive dataset. This translates to more reliable statistics for generating a 3D Discrete Fracture Network (DFN), a stochastic model for fractures within a rock mass, which can be used to estimate the IBSD.

DFNs have been used in wide variety of applications that have brought value to both surface and underground mining operations. In underground operations, DFNs have been used for optimizing stope design to reduce dilution (Urli and Esmaieli, 2016) and in caving operations for fragmentation analysis (Rogers et al., 2015 and Brzovic et al., 2015). In surface operations, DFNs have been useful for assessing blast parameters and viability of quarries for desired dimensions of stone (Latham et al., 2006b, and Yarahmadi et al., 2018). The aforementioned studies use some form of IBSD assessment based on DFN modeling.

The objective of blasting is to reduce the IBSD to a target blasted block size distribution (BBSD), therefore, fragmentation and blast performance are directly affected by the IBSD and jointing. Rock masses with a smaller IBSD and more naturally occurring blocks require less blast energy to obtain the BBSD (Scott, 1996). Figure 1 describes the typical blasting process for rock fragmentation.

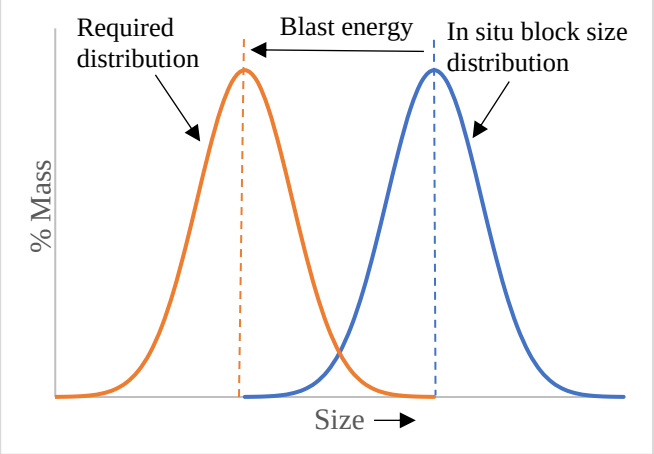

Fig. 1. Fragmentation process after Scott, 1996.

This paper presents a case study conducted at the McEwen mining's El Gallo mine in Sinaloa, Mexico. The study presents the application of a UAV system for pit wall mapping, development of a DFN model to estimate the ISBD, using a UAV system for estimation of BBSD, and comparison of the ISBD and BBSD to estimate the blast energy used for block size reduction. The focus of this study was the analysis of the north eastern wall of the Lupita pit. This area was identified by site personnel as an area of geotechnical concern. Remote sensing of the pit wall and a blasted muck pile was done using the UAV platforms, DJI Matrice 600 Pro and DJI Phantom 4 Pro. Both photogrammetry and Lidar remote sensing techniques were performed in the field. The pit wall data collected remotely was used to supplement the field mapping done by geotechnical consultants, Call and Nicholas Inc. (CNI), (2016). Using the joint mapping data, a DFN model was generated to obtain the ISBD. The fragmentation analysis based on photogrammetry was conducted to obtain the BBSD. Finally, the IBSD and BBSD were compared and the results presented.

2. METHODOLOGY

The following section describes the method used for collecting data during field testing and the data used for the generation of a DFN model.

2.1. Equipment Used

As mentioned previously, the DJI Matrice 600 Pro and the DJI Phantom 4 Pro were selected as the UAVs to carry out the experiments. The DJI Matrice 600 Pro was selected due to high payload capacity and ability to be integrated with LiDAR equipment. The DJI Ronin MX was used for mounting and as a power source for a Velodyne Puck LITE LiDAR. The DJI Phantom 4 Pro was used due to its high resolution camera and its availability as a spare UAV for data collection. Figure 2 shows the UAV configurations for LiDAR and photogrammetry data collection methods. The initial objective was to collect both LiDAR and photogrammetry data of the pit wall. However, the limitations discussed in Section 4 precluded the use of LiDAR data for the joint set analysis. Figure 3 shows an orthophoto of the pit wall generated by aerial photogrammetry.

2.2. Pit Wall Mapping Data

CNI mapped 46 windows during December 2016 for geotechnical purposes. The original mapping data was obtained, and of these 46 windows, 29 windows were located on the north eastern wall of the Lupita Pit of interest. The locations of the mapping conducted is shown in Figure 4 as red crosses and the UAV flight area is shown in the red box. It should be noted that window mapping was done in December 2016, and the pit has progressed since then. However, windows numbered 50-62 and 20-28 have remained, because they were done on the main ramp walls. The remaining data used represents the same geotechnical domain. The collected data includes:

Fig. 2 DJI Matrice 600 Pro with LiDAR setup (left) and DJI Phantom 4 Pro (right).

Fig. 3 Orthophoto of the north-eastern pit wall looking north.

- Size of the window mapped
- Face dip direction (DipDir) and dip
- Discontinuity type
- Discontinuity DipDir and dip
- Roughness of discontinuity
- Maximum length of discontinuity within a set
- Mean length of discontinuities for each set within window
- Mean spacing of sets within window
- Number of fractures within a window for each individual set

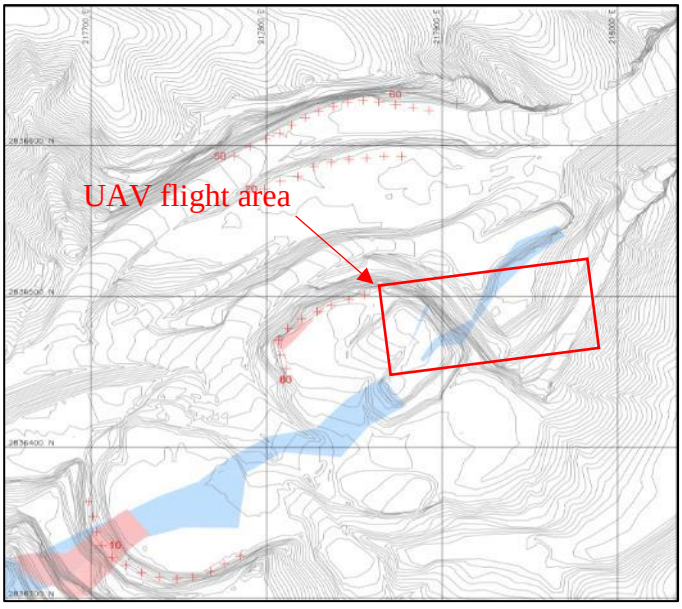

Fig. 4. Location of window mapping and UAV flight area at Lupita Pit.

A coloured 3D point cloud was developed for the area of study using the aerial photogrammetry data (Fig. 5). This allowed identifying joints and major structures on the surveyed pit wall. The geometrical characteristics of the exposed discontinuities were measured. The results of aerial mapping confirmed the window mapping data in terms of geometrical characteristics of discontinuity sets and allowed identifying an additional major structure (a fault zone) in the area of study to be included in the analysis.

The aerial and manual joint data were presented in a stereonet program to identify the joint sets as shown in Figure 6. Table 1 illustrates the orientation of the identified joint sets and the major structures. The K value presents the dispersion coefficient of each joint set. This information was used as input data for DFN generation.

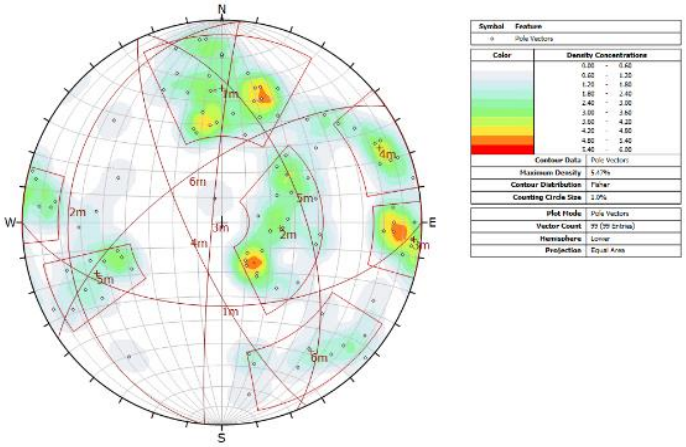

Fig. 6. Stereonet of the joint sets on North Eastern wall.

Fig. 5. Coloured 3D point cloud generated by aerial photogrammetry for wall maping.

Table 1. Orientation of discontinuity data.

Joint Set	DipDir (º)	Dip (º)	Fisher's K
1	180	56	21.7
2	276	24	19.0
3	275	86	36.7
4	245	76	52.4
5	68	57	38.6
6	325	67	24.5
Fault 1	250	75	-
Fault 2	260	07	-

2.3. DFN Generation

The commercially available software *FracMan v.7.6* (Golder 2018) was used to build the DFN model. The reliability of a DFN model greatly depends on the quality of the input data and ensuring the correct joint properties are collected (Elmo et al., 2015). The joint set data identified in Table 1 was used for development of a DFN model. Using the mapping data, it was possible to determin distributions for the trace length of fracture sets and the maximum length of the joints.

Using the trace length of the joints exposed on the bench windows it was possible to calculate the total length of discontinuities for each joint set and calculate the areal fracture intensity (P_{21}) of the set. The DFN model generation was done through an iterative process using the mean trace length and an initial arbitrary volumetric fracture intensity (P_{32}) for each set. Volumetric fracture intensity (P_{32}) cannot be measured directly in the field, however; it's value can be inferred through P_{21} or P_{10} (Esmaieli et al. 2010). Each joint set was generated separately in a large model of 100 m x 100 m x 100 m. A trace plane was introduced into the DFN model, parallel to the orientation of the surveyed pit wall and with the same height as the mine bench. Each generated joint set was then intersected with the trace plane to produce a tracemap of the joints on the wall. The tracemap was used to calculate the P_{21} in the model, and was subsequently compared to the field P_{21}. The input P_{32} was adjusted according to this comparison. This iterative process allowed generation and calibration of the DFN model.

As noted above in Table 1 there were 6 joint sets identified, with two major faults running through the area of interest. The faults were modeled as discrete fractures with persistent lengths in the DFN model. Table 2 presents a comparison between the field data and DFN data in terms of areal fracture intensity (P_{21}) and mean fracture trace length. The results show a good agreement between the field and the simulated data. It is important to note that due to the stochastic nature of a DFN model, a joint set generated with the same parameters may not yield exactly the same results in new iterations.

The resulting stereonet of the joints along the traceplane is presented in Figure 7. Overall the orientation data seems to replicate the results found in the field.

Table 2. Comparison of the field and the DFN results.

Joint Set	Field Data		DFN Data	
	P_{21} (m^{-1})	Trace Length (m)	P_{21} (m^{-1})	Trace Length (m)
1	0.11	2.8	0.14	2.5
2	0.14	2.5	0.16	2.3
3	0.13	3.3	0.12	3.5
4	0.27	3.1	0.24	2.5
5	0.10	3.8	0.11	4.1
6	0.07	1.4	0.06	1.3

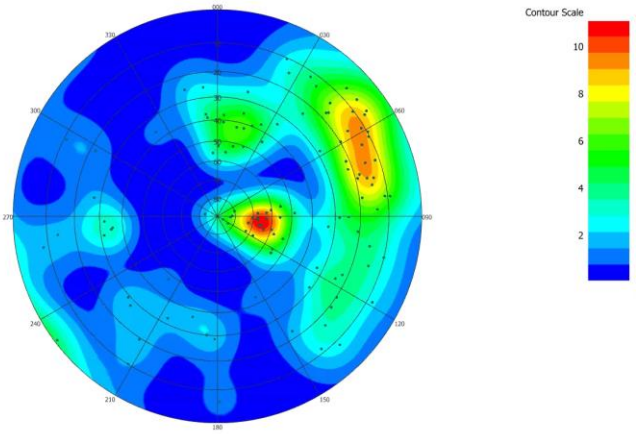

Fig. 7. Stereonet of the joint sets generated by the DFN model on a window map of 15m H x 25m W equivalent to a full bench face.

Fig. 8 shows the generated 100^3 m^3 DFN model. The large blue and cream discrete fracture planes present the major faults in the model. The model was used to estimate the IBSD.

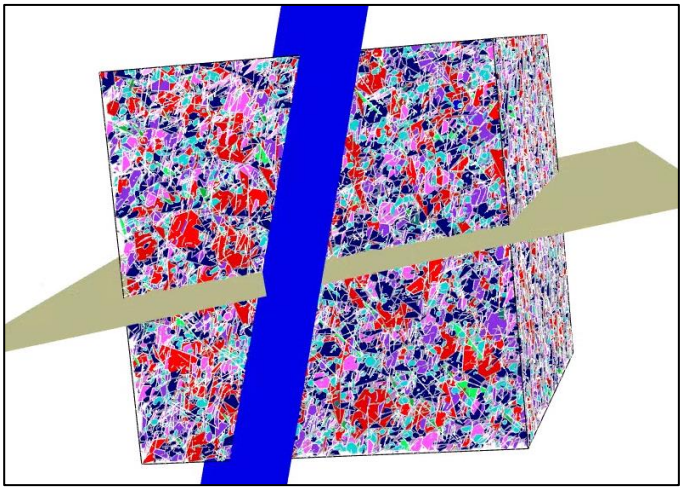

Fig. 8. Developed 3D DFN Model.

2.4. Muckpile Fragmentation Measurement

Many methods have been developed to estimate the BBSD. These methods include visual observation, sieve analysis, and photo (2D) and 3D image analysis. Image analysis techniques for measuring BBSD are commonly used in mining operations because they provide practical, fast, and relatively accurate measurements (Sanchidrián et al., 2009). Thus far, the most common technique to collect images has been to capture photos of the muckpile from the ground using a camera and physical scale objects to measure image scale. This technique has several limitations, as discussed by Sanchidrián et al., 2009. Of these limitations, the imaging system resolution and image segmentation are very important, since both can lead to an inaccurate measurement of BBSD. While application of 3D imaging and analysis methods has eliminated the need for the placement of scale objects and has reduced the error that is created by the uneven shape of the muckpile surface (Onederra et al., 2015, and Campbell and Thurley, 2017), some limitations still exist. These limitations include a significant amount of capturing time for detailed scans, and, in the use of ground-based stations, having fixed capturing locations to avoid smoothing the 3D data.

UAV technology has become a routine tool in many mine operations for aerial surveying and volume calculations. To automate the measurement of BBSD of muckpiles, UAV systems has been developed (Bamford, et al. 2017). This improves the temporal and spatial resolution of the data used to estimate the resulting BBSD after blasting.

In this study, the DJI Phantom 4 Pro was used to collect images for estimating the BBSD. During the study, the DJI Matrice 600 Pro was also used to collect LiDAR data for estimating the BBSD. Results of processing the LiDAR data collected will be presented in future studies. A muckpile created by the bench blast in the north eastern wall of the Lupita pit was chosen for the BBSD estimation. This is the same area where the aerial pit wall mapping was conducted. Figure 9 shows an orthophoto of the muckpile chosen for the BBSD estimation. To collect images for carrying out photogrammetry in OpenDroneMap, 2018, software, a flight mission was created and flown using the DJI Ground Station Pro application. The flight mission was flown to capture the whole area of the pile at a 10 m altitude and used a gimbal pitch angle stabilized at 45° down. This gimbal pitch angle was chosen so that the UAV would be further from the pit wall while covering the rock pile area, which significantly reduced the risk of collision while in flight.

Once images were collected by the UAV, they were used to produce geographic data in OpenDroneMap. This geographic data includes a 3D coloured point cloud, a digital surface model, and an orthophoto. To georeference the geographic data, GPS data logged by the UAV or ground control points with their location in the set of images can be used. Deploying and maintaining a set of visible ground control points on an active muckpile is expensive, logistically complex, and may not be feasible. Due to this complexity, the GPS data recorded in each photo by the UAV was used to georeference the geographic data produced.

The orthophoto produced by the OpenDroneMap was used in image analysis for BBSD estimation because it is a composite of the collected images corrected to have a fixed scale (See Figure 10). This fixed scale, results in the same lack of distortion, as a map of the muckpile. Thus, to only analyze the area of the muckpile in the orthophoto, the orthophoto was cropped to the boundary shown in Figure 9. For BBSD estimation using image analysis, Split-Desktop by Split Engineering LLC., (2018), was used. This software takes an image and delineates rock fragments using image segmentation. To measure the rock sizes, the fixed orthophoto scale are input into the software. Manual editing was used to improve the rock

Fig. 9. Orthophoto produced by OpenDroneMap using a set of images captured by the UAV of the muckpile in the Lupita pit. The boundary of the muckpile is represented by the red polygon.

delineation process. In future work, custom image segmentation algorithms will be implemented to eliminate the manual editing step and to help automate fragmentation measurement.

3. RESULTS

The following section outlines the results of the comparison between the IBSD and BBSD. With these results, it is possible to back-calculate the theoretical required mass of explosive used per volume of rock blasted, known as the powder factor. This can be compared to the powder factor used in the field for an estimate of the efficiency of the blasting parameters.

3.1. IBSD

The IBSD was obtain using the DFN generated as discussed in Section 2.3. For computational ease, first a smaller region (25^3 m^3) within the original DFN model was analyzed for the IBSD calculation (IBSD1). This was followed by calculating the ISBD for the original 100^3 m^3 DFN model (IBSD 2). The results of these are shown in Figure 11. The algorithm run to obtain the block size in *FracMan* was Ray Cast Volume (Dershowitz, 1987).

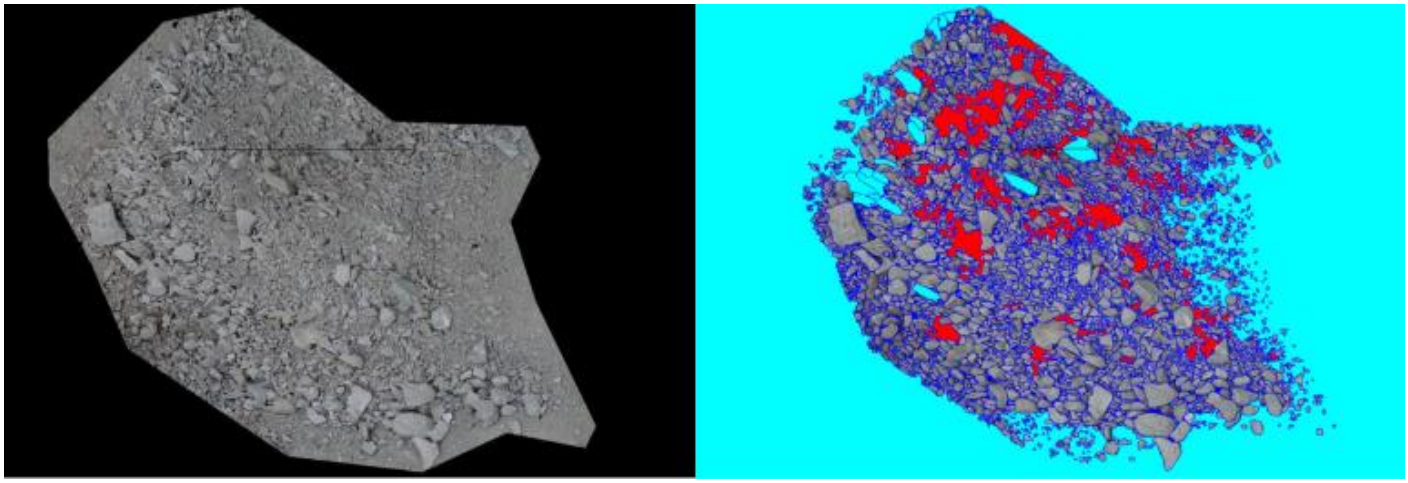

(a) Orthophoto produced by OpenDroneMap. (b) Delineated orthophoto.

Fig. 10: Image analysis of the muckpile using the orthophoto created by OpenDroneMap. In 8b, blue regions represent rock fragment boundaries, light blue regions are masked, and red regions represent fines.

Using this algorithm, random points within the DFN model are used as the origins of rays that are cast out un till they hit a fracture surface. The length of these various rays is sampled a specified number of times and the mean length is used to estimate the volume of the blocks. This algorithm was used due to its simplicity and as it requires the least computation power and time to obtain the results.

The IBSD has an 80% passing size of approximately 6.5 m. Additionally, as can be seen from the results there was a minimal difference between the smaller and larger DFN regions for the IBSD calculation, with almost no discernable difference in passing. The spread of the data is relatively large as well, with most of the block sizes falling between 1.0 m and 10.0 m. This data supports observations in the field that the rock mass is massive and was not blocky as shown in Figure 3.

3.2. BBSD

To measure the BBSD of the muckpile chosen in the north eastern wall of the Lupita pit, an orthophoto was generated by OpenDroneMap from the images collected by the UAV. This orthophoto was generated at a resolution of 80 pixels per meter. Once the orthophoto was cropped, it was imported into Split-Desktop for delineation of rock fragments using image segmentation algorithms and manual editing. Some of the rock fragments in the orthophoto were distorted and had to be manually masked so that they did not introduce error into the resulting BBSD. Figure 10 illustrates the delineation of rock fragments using image segmentation for the chosen muckpile. Figure 11 plots the measured BBSD produced by image analysis for the muckpile.

3.3. Size Distribution Analysis

Comparing the estimated size distributions for IBSD and BBSD it is possible to identify the following:

- Blasting was able to reduce all of the block size within the rock, the largest blasted block is approximately the same size as the smallest in-situ block size (~ 1 m).
- The BBSD represents a larger range of block sizes than the IBSD.
- The 80% passing of the BBSD is approximately 0.37 m compared to 6.5 m in the IBSD.
- At 50% passing – the blasted block size is 2.8% of the in-situ block size and the block size was reduced from 4.5 m to 0.13 m.

At the El Gallo mine the ore rock is mainly composed of quartz stockwork, veins and breccias. Whereas the barren host rocks are propylitically altered andesitic rocks of various grades (CNI, 2016). The typical density of the rock is 2.5 t/m^3. The blast analyzed was a production and pre-shear shot. 40 production holes with 156 mm in diameter were loaded to blast 5,970 tonnes of rock (2,370 m^3 of rock). The holes were loaded using ANFO with a density of 820 kg/m^3. The bench height was approximately 5 m and the holes are sub-drilled 1 m. The loaded length of hole was 3 m and approximately 3 m of stemming was used. The resulting blast had a powder factor of ~0.78 kg/m^3. These values were obtained from the on-site blasting engineers. Latham et al., (2006a) discuss the various relationships between powder factor, the in-situ and blasted block sizes in detail. A recent

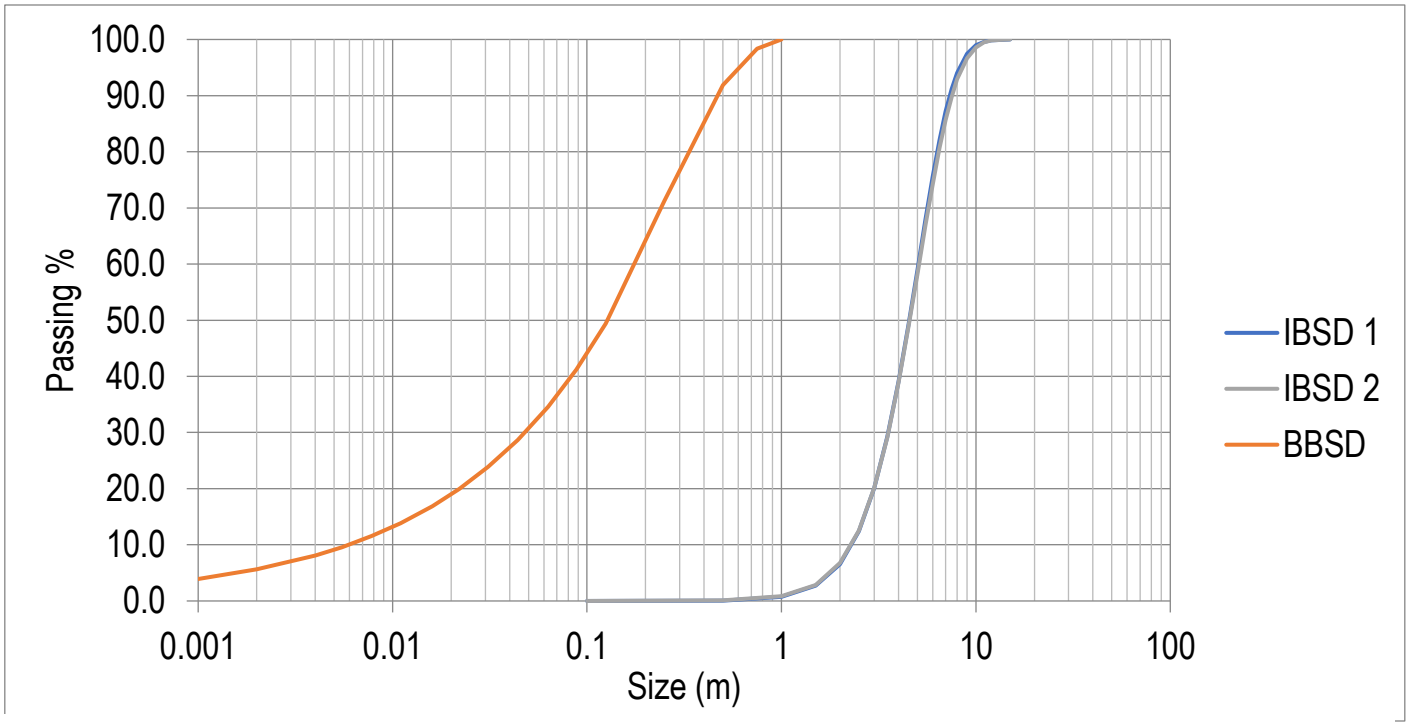

Fig. 11. Graph showing the difference of block size by % passing between the blasted rock (BBSD), and in-situ rock (IBSD)

update by Kahriman et al., 2013 was done on the estimation of the powder factor based on the Bond work index. This work relates the powder factor (q_B) through the relationship in equation 1.

$$q_B = 10\, W_i \left\{ \left(\frac{1}{\sqrt{D_{b80}}} \right) - \left(\frac{1}{\sqrt{D_{i80}}} \right) \right\} K \qquad (1)$$

Where W_i is the Bond's work index calibrated, D_{b80} and D_{i80} are 80% passing for BBSD and IBSD respectively (in micrometer). K is a conversion constant relating the energy in used in Bond's work index to the energy in ANFO and the specific gravity of the rock.

$$K = (860/912) \times \rho_r. \qquad (2)$$

A W_i of 16.3 was obtained from the resource estimate report for the El Gallo Complex, (2013), by McEwen Mining. Using this model, the expected powder factor for the investigated blast is 0.47kg/m^3. This is 40% lower than the actual powder factor used in the blast. This indicates that significant amount of blast energy was lost. This energy could have resulted in additional ground vibrations, gas, over-break into the catch benches, and damage of the final wall. This was observed in the field where the catch benches were narrower than design, and blast damage was identified in the final pit walls. Information such as this can lead to optimization of the blasting process, or at least bring about useful site discussions on potential improvements for operations.

4. DISCUSSION

Using the DFN approach it is possible to gain a better understanding of the in-situ rock mass block size. However, similar to other types of models, a DFN has to be calibrated to reflect the actual field conditions. A strong understanding of the input parameters in a DFN could act as a guide for features that are important for field mapping, thereby increasing the accuracy of the DFN (Elmo et al., 2014). Using aerial mapping techniques with UAV allows covering a large area of pit slope and thus improves the statistics of the input parameters in developing a DFN model. This can increase the reliability of the results obtained from the DFN model. Moreover, once the DFN was generated, it can be leveraged for a kinematic analysis of the pit to identify areas of risk.

It should be noted that the original objective of the case study was to use both LiDAR and photogrammetry data collected by the UAV for the analysis of the joint sets. However, some limitations of the experimental design and equipment reliability prevented the successful completion of this objective. The LiDAR scanning was ineffective because of noise related to GPS positioning, sudden maneuvers in the flight plans of the UAV, and the speed and orientation of the LiDAR scan. These issues will be addressed in future work by reducing the speed and optimizing flight plans to eliminate any rotations or sudden maneuvers.

5. CONCLUSION

The use of UAVs can aid with real-time mining data collection and mine monitoring while decreasing personnel exposure to hazards. This increased access to data can be beneficial in the timely relay of field data to mine site personnel and allows for detailed tracking of performance without significantly impacting the time required to do so. It is possible to fly a UAV over a muckpile while the shovel is digging, thereby avoid work interruption. In this regard, the case study used a UAV to effectively map a blasted muck pile while minimizing exposure and time in the field. It also enabled the remote sensing of a larger pile from a better angle than traditional ground-based techniques. The use of UAV allowed a significant area to be mapped for the photogrammetry, increasing the availability of the data for digital discontinuity mapping. This was used to supplement field mapping done. The photogrammetry allowed for the analysis and visual inspection of areas of the pit wall that were previously inaccessible. This advantage is particularly valuable in areas where potential failures have been identified and the pit mining progresses deeper, eliminating access to these areas.

Overall, the case study demonstrates the potential for use of a DFN along with the UAV technology for integration of remotely sensed data into an operating mine. The generation of the block size distributions obtained in the case study can assist with the improvement of blasting processes in the mine. The blasted rock size data was fully obtained through the use of remote sensing which was executed in the field in less than an hour. Similarly, the photogrammetry was conducted in a single morning. While the field component was relatively quick, the post-processing required more time and was relatively manual due to some of the limitations discussed in the paper. This is the focus of our future work, to increase the post-processing speed and increase the automation of these process. These improvements would enable on-site personnel to focus on more important aspects; data interpretation and using the data correctly, rather than collecting the data itself.

ACKNOWLEDGEMENTS

The authors would like to thank the financial support by McEwen Mining Inc. and the Natural Sciences and Engineering Research Council of Canada (NSERC).

REFERENCES

Bamford, T., K. Esmaieli, and A. P. Schoellig. 2017. A real-time analysis of post-blast rock fragmentation using UAV technology. *International Journal of Mining, Reclamation and Environment* 31:6 439-456.

Brzovic, A., S. Rogers, G. Webb, J. P. Hurtado, N. Marin, P. Schachter, J. Alvarez, and K. Baraona. 2015. Discrete fracture network modelling to quantify rock mass pre-conditioning at the El Teniente Mine, Chile. *Mining Technology* 124:3 163-177.

Call & Nicholas INC. 2016. Slope Recommendations for the Lupita mining area.

Campbell, A. D. and M. J. Thurley. 2017. Application of laser scanning to measure fragmentation in underground mines. *Mining Technology* 126:4 240–247.

Dershowitz, W. S. and H. H. Einstein. 1988. Characterizing rock joint geometry with joint system models. *Rock Mechanics and Rock Engineering* 21: 21-51.

Elmo, D., S. Rogers, D. Stead, and E. Eberhardt. 2014. Discrete fracture network approach to characterise rock mass fragmentation and implications for geomechanical upscaling. *Mining Technology* 123:3 149-161.

Elmo, D., D. Stead, and S. Rogers. 2015. Guidelines for the quantitative description of discontinuities for use in discrete fracture network modelling. In *Proceedings of the 13th ISRM Int'l Congress of Rock Mechanics, 10-13 May, Montreal, Canada*, 1-11.

Elmouttie, M. K. and G. V. Poropat. 2012. A method to estimate in situ block size distribution. *Rock Mechanics and Rock Engineering* 45:3 401-407.

Esmaieli, K., J. Hadjigeorgiou, and M. Grenon. 2010. Estimating geotechnical and mechanical REV, based on synthetic rock mass models at Brunswick Mine. *Int. J. Rock Mechanics and Mining Science*, 47:6 915-926.

Grenon, M., J. Hadjigeorgiou, and Q. Liu. 1998. Quantifying in-situ rock block size and resulting fragment size distributions due to blasting. *Int'l J. for Blasting and Fragmentation* 2:2 205-218.

Golder Associates Ltd. 2018. FracMan

Kahriman, A., Ş. G. Özkan, Ö. L. Sül, and A. Demirci. 2001. Estimation of the powder factor in bench blasting from the Bond work index. *Mining Technology* 110:2 114-118.

Latham, J., J. V. Meulen, and S. Dupray. 2006a. Prediction of fragmentation and yield curves with reference to armourstone production. *Engineering Geology* 87: 60-74.

Latham, J., J. V. Meulen, and S. Dupray. 2006b. Prediction of in-situ block size distributions with reference to armourstone for breakwaters. *Engineering Geology* 86: 18-36.

Onederra, I., M. J. Thurley, and A. Catalan. 2015. Measuring blast fragmentation at Esperanza mine using high-resolution 3d laser scanning. *Mining Technology* 124:1 34–36.

OpenDroneMap Org.. 2018. OpenDroneMap: Open source toolkit for processing aerial drone imagery.

Read, J., and L. Willis. 2013. Resource Estimate for the El Gallo Complex, Sinaloa State, Mexico. *McEwen Mining*.

Rogers, S., D. Elmo, G. Webb, and A. Catalan. 2014. Volumetric fracture intensity measurement for improved rock mass characterisation and fragmentation assessment in block caving operations. *Rock Mechanics and Rock Engineering* 48: 633-649.

Sanchidrián, J. A., P. Segarra, F. Ouchterlony, and L. M. López. 2009. On the accuracy of fragment size measurement by image analysis in combination with some distribution functions. *Rock Mechanics and Rock Engineering* 42:1 95–116.

Scott, A. 1996. Blastability and blast design. In *Proceedings of Fragblast '96, Montreal, Canada*: 27-35. Rotterdam: Balkema.

Split Engineering LLC.. 2018. Split-Desktop: Fragmentation analysis software.

Urli, V. and K. Esmaieli. 2016. A stability-economic model for an open stope to prevent dilution using the ore-skin design. *Int'l J. of Rock Mechanics and Mining Engineering* 82: 71-82.

Yarahmadi, R., R. Bagherpour, S. Taherian, L. M. O. Sousa. 2018. Discontinuity modelling and rock block geometry identification to optimize production in dimension stone quarries. *Engineering Geology* 232: 22-33.